

## Article

# Effect of Mesoporous Chitosan Action and Coordination on the Catalytic Activity of Mesoporous Chitosan-Grafted Cobalt Tetrakis(p-Sulfophenyl) Porphyrin for Ethylbenzene Oxidation

Guan Huang <sup>\*</sup> , Lin Qiang Mo, Yan Xun Wei, Hong Zhou, Yong An Guo and Su Juan Wei

Guangxi Colleges and Universities Key Laboratory of Applied Chemistry Technology and Resource Development, College of Chemistry and Chemical Engineering, Guangxi University, Nanning 530004, Guangxi, China; molinjiangw@163.com (L.Q.M.); weiyanyun@163.com (Y.X.W.); zhoujong1964@126.com (H.Z.); guoyong\_an@126.com (Y.A.G.); wsj64913@126.com (S.J.W.)

\* Correspondence: huangg66@126.com or huangg66@gxu.edu.cn;  
Tel.: +86-771-3237-868; Fax: +86-771-2851-043

Received: 10 April 2018; Accepted: 4 May 2018; Published: 10 May 2018



**Abstract:** To simulate the active site cavity structure function and axial coordination of cytochrome P-450 enzymes, mesoporous chitosan(mesp-CTS) was used as a scaffold for a meso-sized cavity to immobilize cobalt tetrakis(p-sulphophenyl)porphyrin chloride(Co TPPS). Immobilization was achieved via an acid–base reaction and axial coordination of the H<sub>2</sub>N-C group to the Co ion in Co TPPS, thus forming the biomimetic catalyst Co TPPS/mesp-CTS. Several approaches, including scanning electron microscopy (SEM), the Brunauer–Emmett–Teller (BET) technique, Fourier transform infrared (FT-IR) spectroscopy, ultraviolet-visible (UV-vis) spectroscopy, thermogravimetric and differential scanning calorimetry (TG-DSC), and X-ray photoelectron spectroscopy (XPS), were used to characterize the grafted catalyst. The catalytic performance of Co TPPS/mesp-CTS in ethylbenzene oxidation without any solvents and additives was investigated. The results showed that only  $0.96 \times 10^{-4}$  mol of Co TPPS grafted onto mesp-CTS could be recycled three times for 200 mL of ethylbenzene oxidation, with an average yield of 44.6% and selectivity of 68.8%. The highly efficient catalysis can be attributed to promotion by mesp-CTS, including the effect of the mesoporous structure and the axial coordination to the Co ion in Co TPPS. This biomimetic methodology provides a method for clean production of acetophenone via ethylbenzene oxidation.

**Keywords:** mesoporous chitosan; cobalt porphyrin; acetophenone; ethylbenzene oxidation

## 1. Introduction

Methods for achieving highly efficient oxidation of ethylbenzene in high-value added products, acetophenone and 1-phenylethanol, are very welcome in the chemical industry. Recently, the oxidation of ethylbenzene has been optimized to produce high yields of acetophenone [1–10]. During the production of high-value added products, however, there are many requirements that have to be met. For example, the catalyst should be highly effective and recyclable [4], and should not produce toxic by-products, while the oxidant should be eco-friendly and sustainable [3,5]. Furthermore, the catalytic oxidation system should eliminate the use of solvents [5], the oxidation time should be as short as possible [5], and the potential for explosions of the oxidation reaction at high temperatures and pressures, even at room temperature, should be minimized [11]. To meet these requirements, some scientists have technically employed the microstructured reactor successfully to solve the potentially explosive problem, and the microreactor technique has been used to enhance the production rates

of the hydrocarbon (alkylideneoxazoles and cyclohexane) oxidation with  $O_2$  [11,12] and an aqueous solution of  $H_2O_2$  [13], respectively; many investigators have also designed catalysts with excellent properties, which were tested in various oxidation systems to investigate their catalytic effects. Many of these catalysts were associated with several advantages, as well as disadvantages, with regard to oxidation systems [1–10,14–17]. In most cases, the inability to satisfy the five criteria listed above greatly limits their practical applications. Therefore, designing the best catalyst for the oxidation of ethylbenzene to acetophenone remains a challenge.

Enzyme and biomimetic catalysts are useful in society because they are environmentally friendly. Immobilized metaloporphyrins are biomimetic catalysts that have gained popularity because of their distinctive catalytic activities and stability [18–21]. In addition, polymer-supported metaloporphyrins have several advantages over conventional homogeneous catalysts because of the steric and electronic effects of the supports, which in some respects are analogous to the influence of the polypeptide chain in hemoproteins [22,23]. Many studies have attempted to mimic the cavity function and axial coordination of cytochrome P450 enzymes using different metaloporphyrins with carrier cavities and various axial ligands, which affected the catalytic activities of the metaloporphyrins [24,25], as well as their product selectivities [26]. Previously reported models attempting to mimic cytochrome P450 enzymes possessed rather variable catalytic behavior, and thus producing efficient, stable P450 mimics remains challenging.

Based on the considerations described above, we have investigated the oxidation of ethylbenzene over powdered chitosan(pd-CTS)-supported manganese tetrakis(4-carbonylphenyl) porphyrin(Mn TCPP/pd-CTS), nanoporous chitosan(np-CTS)-supported manganese tetrakis(4-carbonylphenyl) porphyrin (Mn TCPP/np-CTS), and powdered chitosan(pd-CTS)-supported cobalt tetrakis(4-carbonylphenyl) porphyrin (Co TPPS/pd-CTS), and found that the yields (one + ol) were 13.2% averaged over three runs [27], 13.8% averaged over five runs [28], and 13.5% averaged over eight runs [29], respectively. A comparison of the catalytic activity of Mn TCPP/pd-CTS with that of Mn TCPP/np-CTS revealed that the latter gave higher ethylbenzene conversion (24.5 mol %) under reaction conditions of 145 °C and 0.8 MPa, in comparison with the former (20.7 mol %) under reaction conditions of 155 °C and 0.8 MPa. This finding indicates that np-CTS improved the catalytic performance of Mn TCPP more effectively than pd-CTS. However, the selectivity (one + ol) of Mn TCPP/np-CTS (69.7%) was lower than that of Mn TCPP/pd-CTS (85.5%). This led us to predict that the chitosan-mesoporous action and the coordination to metaloporphyrins will improve the yields of the main products (one + ol), thus we investigated the effects of each of these factors on selectivity with regard to the corresponding ketone and alcohol.

In this study, to improve the selectivity and yield of acetophenone and 1-phenylethanol production, we developed a novel mesoporous chitosan-grafted cobalt tetrakis(p-sulfophenyl)porphyrin (Co TPPS/mesp-CTS) to catalyze the oxidation of ethylbenzene. The goal of this approach was to develop and expand our previous studies [27–29] on the effect of chitosan's cavity and axial coordination on the catalytic activity of mesoporous chitosan-grafted cobalt tetrakis(p-sulfophenyl)porphyrin for ethylbenzene oxidation, with the aim of understanding how the characteristics of chitosan promote the catalytic activity of Co TPPS.

## 2. Experimental Section

### 2.1. Chemicals

All chemicals and solvents were of analytical grade, obtained commercially, and used as received without further purification. Powdered chitosan (MW,  $\sim 7.7 \times 10^4$  Da; degree of deacetylation, 90.3%) was purchased from Zhejiang Jinke Biochemistry Co., Ltd. (China). Deionized water was made in our laboratory.

## 2.2. $H_2$ TPPS and Co TPPS Synthesis

Tetrakisphenylporphyrin ( $H_2$  TPP) was prepared as described previously [30]. In brief, a propionic acid solution of pyrrole and benzaldehyde was refluxed for 40 min in nitrogen, and cooled slowly to room temperature. The resulting crystallites of tetrakisphenylporphyrin were filtered, sequentially washed with ethanol and water, and dried for further use.

Tetrakis(p-sulphophenyl)porphyrin [ $H_2$  T(p-SO<sub>3</sub>H)PP], designated as  $H_2$  TPPS, was synthesized as described previously with minor modifications [31]. Two milliliters of freshly redistilled chlorosulfonic acid was added drop-wise into a mixture of 15 mL chloroform solution and 0.75 g  $H_2$  TPP with stirring, and the mixture was heated at 30 °C for 1 h. To decompose the excess chlorosulfonic acid, the resulting solution was poured slowly into ice water. The water evaporated and  $H_2$  TPPS was allowed to dry, resulting in the formation of dark green crystals (1.04 g).

Cobalt tetrakis(p-sulphophenyl)porphyrin (Co TPPS) was synthesized as described previously with minor modifications [31]. First, 0.3 g of  $H_2$  TPPS was dissolved in 70 mL of deionized water, the mixture was refluxed, 0.1 g of hydrate cobalt chloride (CoCl<sub>2</sub>·6H<sub>2</sub>O) was added, and the mixture was stirred for 1.5 h. The process of metalation was monitored by following the change of the Soret bands from  $H_2$  TPPS to Co TPPS. After evaporation of the solvent, the resulting solid was recrystallized with a mixture of methanol/water (v:v, 1:1). Thereafter, cobalt complex Co TPPS was purified by silica column chromatography, using methanol as the elutant. A reddish-brown solid (0.2 g) was obtained after evaporation of the methanol.

## 2.3. Preparation of Co TPPS/mesp-CTS Catalyst Material

Chitosan beads were prepared as described previously [32]. A mixture of 7.5 g of pd-CTS and 380 mL of acetic acid (3.9 wt %) was stirred vigorously for 12 h. The resulting chitosan-gelatinous solution was added drop-wise to a 10% NaOH solution, forming many small, white chitosan-balls. The chitosan-balls were washed and soaked in water until the water was neutral. The neutral white chitosan-balls were added to 1500 mL of glutaraldehyde solution (2.5 wt %) and cross-linked for 12 h. The white cross-linked chitosan-balls were rinsed extensively with water to remove all traces of glutaraldehyde. Thereafter, a portion of the white chitosan-balls was freeze-dried for 36 h to yield mesoporous CTS microspheres (mesp-CTS, mean pore diameter of 2–50 nm and mean ball diameter of 3–4 mm, Figure 1), while another portion was dried under a vacuum at 80 °C for 24 h to yield macroporous-CTS (macp-CTS, mean pore diameter larger than 50 nm and mean ball diameter of 3–4 mm, Figure 1).

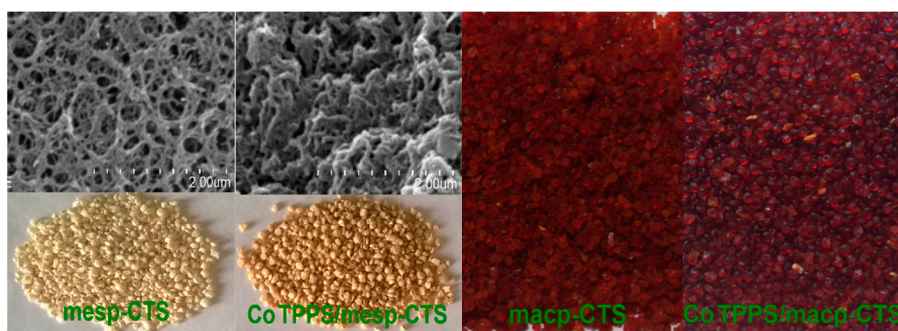


**Figure 1.** Images of mesoporous chitosan (mesp-CTS), cobalt tetrakis(p-sulphophenyl)porphyrin chloride (Co TPPS)/mesp-CTS, macroporous-CTS (macp-CTS) and Co TPPS/macp-CTS; scanning electron microscopy (SEM) images of mesp-CTS and Co TPPS/mesp-CTS.

A 10-mL sample of Co TPPS solution (30 mg) was added slowly to a 250-mL suspension of mesp-CTS microspheres (30 g) with gentle stirring over 1 h at room temperature. The resulting microspheres were filtered and dried under a vacuum at 55 °C for 6 h to yield Co TPPS/mesp-CTS. The content of

cobalt tetrakis(p-sulphophenyl)porphyrin in the filtrate was determined by ultraviolet-visible (UV-vis) spectroscopy [33]. The content of grafted cobalt tetrakis(p-sulphophenyl)porphyrin in the microspheres was determined by inductively coupled plasma atomic emission spectroscopy (ICP-AES Spectroflame model FVMØ3). The sample was digested using a traditional acid method (HNO<sub>3</sub> and HCl), diluted adequately, and analyzed for cobalt. The content of grafted Co TPPS per gram of mesp-CTS microspheres was 1.02 mg, which was consistent with that determined by UV-vis spectroscopy [33]. Co TPPS/macp-CTS was prepared using a similar method, and the content of grafted Co TPPS per gram of macp-CTS was 1.01 mg.

#### 2.4. Characterization Equipment

Scanning electron microscopy (SEM) images were obtained with a S-3400 scanning electron microscope. Nitrogen adsorption/desorption measurements were carried out on a Gemini VII porosimetry analyzer. The specific surface area and pore size distribution were calculated by Brunauer–Emmett–Teller (BET) and BJH(Barrett-Joyner-Halenda) methods, respectively. IR spectra were obtained with a Nexus 470 Fourier transform infrared (FT-IR) spectrophotometer using the KBr disk method in the range of 400–4000 cm. UV-vis spectra were obtained with a TU-1810SPC spectrophotometer in the range of 300–700 nm, and analyses were performed with a 1-cm path length cell. Thermogravimetric and differential scanning calorimetry (TG-DSC) was conducted on a STA 409 PC/PG Luxx thermo analyzer in an atmosphere of air with a flow rate of 20 mL per min. X-ray photoelectron spectrometry (XPS) was conducted on a Kratos Ultra Axis DLD photoelectron spectrometer using a monochromatic Al K<sub>α</sub> radiation source with a pass energy of 40 eV.

#### 2.5. Measurement of Catalytic Performance for Co TPPS/Mesp-CTS

Catalytic oxidation of ethylbenzene was carried out in a 0.25-L autoclave reactor equipped with a magnetic stirrer and a frozen ethanol recondenser at −20 °C [34]. In brief, the substrate (200 mL) and catalyst (0.97 × 10 mol Co TPPS) were added to the reactor. The reaction was performed at a specific temperature (130–150 °C). When the reaction reached the required temperature, O<sub>2</sub> was continuously bubbled into the autoclave at the desired pressures (0.6–1.0 MPa). During the 4-h oxidation reaction, samples were drawn at 30-min intervals and analyzed/quantified by gas chromatography-mass spectrometry (GC-MS), using a Shimadzu GC-16A chromatograph equipped with a 30 m × 0.32 mm × 0.5 µm FFAP capillary column and a flame ionization detector. Bromobenzene was used as the internal reference. To study the reuse potential of the chitosan-grafted metalloporphyrin materials, the catalysts were separated from the reaction mixture after the reaction was terminated, washed in ethanol, air-dried to remove residual oxidation products, and used for oxidation of ethylbenzene.

### 3. Results and Discussion

#### 3.1. Characterization for the Co TPPS/mesp-CTS Material

Figure 1 shows images of mesp-CTS, Co TPPS/mesp-CTS, macp-CTS, and Co TPPS/macp-CTS. The slight color change from the various supports after grafting to the corresponding materials indicates that Co TPPS grafted to mesp-CTS and macp-CTS. When the acid–base reaction was used to graft Co TPPS to CTS, Co TPPS molecules rarely aggregated together. Although there were apparent differences in the microstructure of Co TPPS/mesp-CTS and mesp-CTS by SEM (Figure 1), there were only slight differences in the specific surface areas and adsorption average pore diameters of Co TPPS/mesp-CTS and mesp-CTS. In addition, the BET adsorption isothermal lines of Co TPPS/mesp-CTS and mesp-CTS were identical and similar, respectively, to the III type (Figure 2). However, the BET adsorption isothermal lines of Co TPPS/macp-CTS and macp-CTS were more similar to the II type, and rather different from those of Co TPPS/mesp-CTS and mesp-CTS (Figure 2). Therefore, Co TPPS/macp-CTS and macp-CTS both possessed macroporous structures (Figure 1). Our results indicate that the BJH pore-size distributions of Co TPPS/mesp-CTS and mesp-CTS were similar. The average pore diameters

of Co TPPS/mesp-CTS and mesp-CTS were approximately 23 nm (Table 1). We predicted that the catalytic performance of Co TPPS/mesp-CTS would be better than that of Co TPPS/macp-CTS [35].

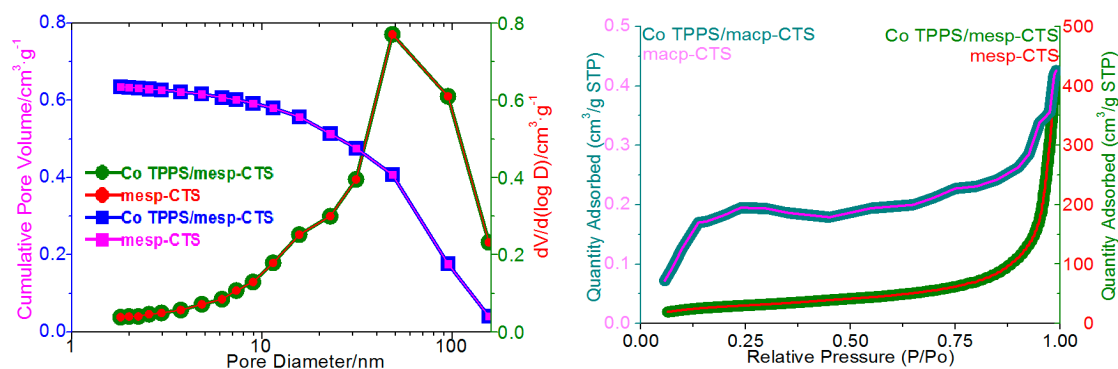


**Figure 2.** BJH pore-size distribution of Co TPPS/mesp-CTS, mesp-CTS; BET adsorption isothermal plot of Co TPPS/mesp-CTS, mesp-CTS, Co TPPS/macp-CTS and macp-CTS.

**Table 1.** Physical characteristics of mesoporous chitosan (mesp-CTS) and cobalt tetrakis (p-sulphophenyl)porphyrin chloride(Co TPPS)/mesp-CTS. BET; BJH.

Material	BET Surface Area (m/g)	BJH Total Pore Volume (cm/g)	BJH Adsorption Average Pore Diameter (nm)
mesp-CTS	104.2	0.64	23.1
Co TPPS/mesp-CTS	102.2	0.64	23.0

Figure 3A shows the FT-IR spectra of pd-CTS, mesp-CTS, Co TPPS, and Co TPPS/mesp-CTS. For pd-CTS, the peaks at 3370 cm and 1596 cm were assigned to the stretching vibration of amino groups, and the peak at 1654 cm was attributed to the carbonyl stretching vibration of the secondary amide [36,37]. The peak at 3370 cm was attributed to the hydroxyl group of chitosan. After chitosan was cross-linked with glutaraldehyde to form mesp-CTS, the intensities of the peaks at 3370 cm and 1596 cm decreased. The formation of a C=N bond between chitosan and glutaraldehyde caused the change in the carbonyl stretching vibration to be minor. For Co TPPS, the peak at 3438 cm was attributed to the stretching vibration of the hydroxyl groups in SO<sub>3</sub>H. The peaks at 1635, 1398, 1039, and 1006 cm were assigned to the porphyrin skeletal modes, while the peaks at 1180 and 1127 cm were vested in sulfonic acid group vibrations. The peak at 640 cm<sup>−1</sup> was assigned to the in-plane-deformation vibration of the pyrrolyl and phenyl groups [38]. When Co TPPS was grafted onto mesp-CTS, thus forming Co TPPS/mesp-CTS, a peak appeared at 3413 cm that was narrower than that of Co TPPS, but slightly larger than that of mesp-CTS. This was because of the acid–base reaction between the sulfonic acid groups of Co TPPS and the amino groups of mesp-CTS, which broke the hydrogen bond in Co TPPS. The acid–base reaction was also supported by the initial peak at 1180 cm in the FT-IR spectrum of Co TPPS, which was absent from that of Co TPPS/mesp-CTS. Instead, two new peaks appeared at 1259 and 1072 cm [39]. It is possible that the peak at 1069 cm in the FT-IR spectrum of mesp-CTS may have contributed to the peak at 1072 cm.



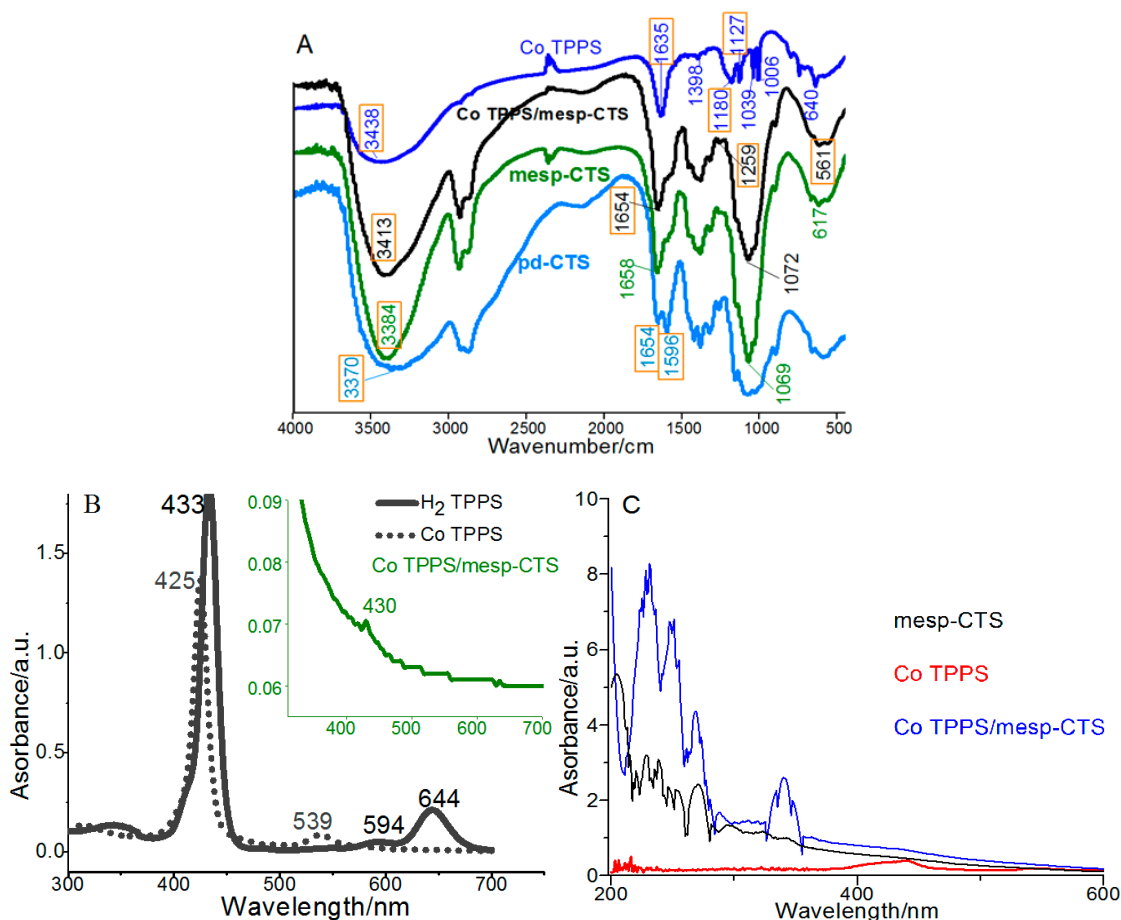


**Figure 3.** (A) Fourier transform infrared (FT-IR) spectra of Co TPPS/mesp-CTS (or Co TPPS/macp-CTS), Co TPPS, mesp-(or macp-)CTS and, powdered chitosan (pd-CTS), with an effective frequency range of 400–4000 cm; (B) ultraviolet-visible(UV-vis) spectra of an aqueous solution of H<sub>2</sub> TPPS ( $\epsilon = 5.3 \times 10 \text{ L}\cdot\text{mol cm}$ ) and Co TPPS ( $\epsilon = 2.7 \times 10 \text{ L}\cdot\text{mol cm}$ ) and an aqueous suspension of Co TPPS/mesp-CTS(or Co TPPS/macp-CTS) ( $\epsilon = 0.4 \times 10 \text{ L}\cdot\text{mol cm}$ ); and (C) UV-DRS (vis diffuse reflectance spectra) spectra of mesp-CTS(or macp-CTS), Co TPPS, and Co TPPS/mesp-CTS (or Co TPPS/macp-CTS).

The reaction between Co TPPS and mesp-CTS was further verified by UV-vis analysis (Figure 3B). For H<sub>2</sub> TPPS and Co TPPS, Soret bands were observed at 433 and 425 nm, respectively; the Q bands of H<sub>2</sub> TPPS appeared at 594 and 644 nm [40], but that of Co TPPS appeared at 539 nm. A blueshift of the Soret band and Q band occurred, indicating that the Co ion of CoCl<sub>2</sub>·4H<sub>2</sub>O coordinated with the H<sub>2</sub> TPPS free base to form Co TPPS [18]. The Soret and Q bands in Co TPPS/mesp-CTS (or macp-CTS), Co TPPS, and mesp-CTS (or macp-CTS) were consistent with previously published reports [41]. When Co TPPS was grafted onto mesp-CTS, the Soret band of Co TPPS at 425 nm shifted to 430 nm (Figure 3B). This shift to the red region of the spectrum is similar to the result of axially coordinating the nitrogen atom in the supports to the cobalt porphyrins [18,41]. As a result of the low amount of metalloporphyrins grafted onto the surface support, the Soret peak height of Co TPPS/mesp-CTS was markedly lower than that of Co TPPS. In comparison with Co TPPS, the Soret band of Co TPPS/mesp-CTS exhibited a small redshift (ca. 5 nm). This phenomenon suggests that the axial coordination of these ligands to metalloporphyrins resulted in a shift in metal electron density [42].

The UV-DRS spectrum of Co TPPS/mesp-CTS was different from that of Co TPPS and mesp-CTS (Figure 3C), indicating that Co TPPS was grafted onto mesp-CTS. This difference was present because the sulfonyl groups in Co TPPS reacted with the amino groups in mesp-CTS.

The electron cloud densities (ECDs) of the elements on the surface of the Co TPPS/mesp-CTS catalyst, especially that of cobalt, were changed to different degrees after Co TPPS was immobilized on mesp-CTS. Table 2 and Figure 4 show the binding energies (BEs) of key elements in Co TPPS/mesp-CTS, Co TPPS, and mesp-CTS.

There were two BE peaks at 782.1 and 797.6 eV that corresponded to Co 2p<sub>3/2</sub> and Co 2p<sub>1/2</sub>, respectively, for Co TPPS, indicating the presence of Co [43]. There was one major BE peak at 798.0 eV, indicating the presence of Co [44] (Figure 4). After Co TPPS was grafted onto mesp-CTS (or macp-CTS), the BE peaks of Co 2p<sub>3/2</sub> and Co 2p<sub>1/2</sub> in Co TPPS/mesp-CTS (or macp-CTS) increased from 782.1 and 797.6 eV to 786.6 and 798.0 eV, respectively. The BE peak of Cl in Co TPPS at 199.6 eV shifted to 196.4 eV after Co TPPS/mesp-CTS (or macp-CTS) was formed. Additionally, there were two BE peaks at 398.6 and 399.9 eV for Co TPPS, as well as two BE peaks at 398.0 and 399.8 eV for Co TPPS/mesp-CTS (or macp-CTS), which were in accordance with a previous study reporting that the pyrrolic and iminic nitrogens in the porphyrin ring were found between 398–400 eV [45]. The electron BE peak of N 1s in the H<sub>2</sub>N– group unit in mesp-CTS (or macp-CTS) was found at 397.7 eV. However, when mesp-CTS (or macp-CTS) was grafted to cobalt porphyrin, the peak shifted to 398.1 eV. This finding was indicative of axial coordination of lone-pair electrons from the H<sub>2</sub>N– unit to the Co ion in Co TPPS [46]. The BEs shown in shown in Table 2 correspond well with those in previous reports [47–53].

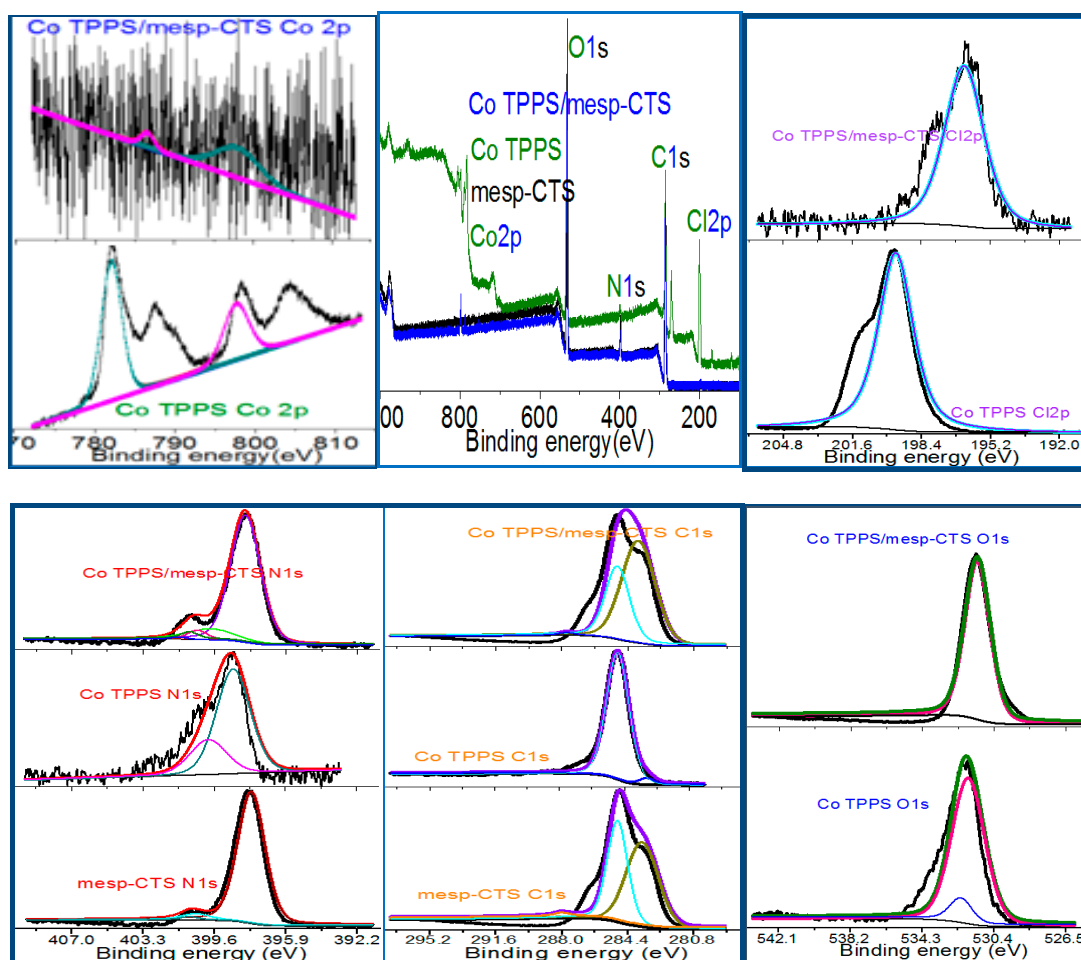


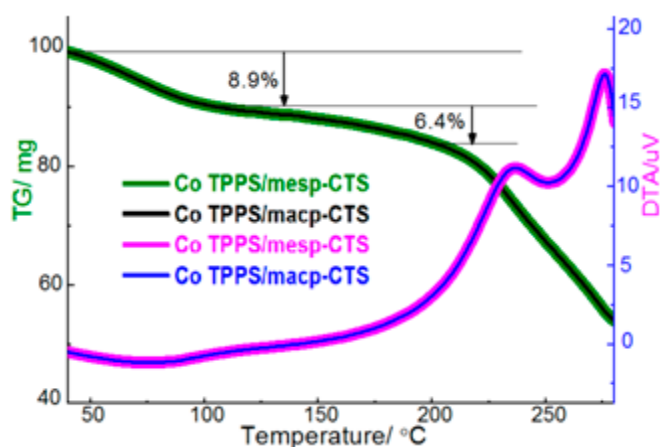
**Figure 4.** X-ray photoelectron spectra and main spectral bands based on the binding energy (BE) of the key elements (Co, Cl, N, and O) for Co (TPPS), Co (TPPS)/mesp-CTS, and mesp-CTS.

**Table 2.** Binding energies of key elements. X-ray photoelectron spectroscopy (XPS).

XPS Spectra	Existential form of the Key Element	Binding Energy/eV		
		Co TPPS/mesp-CTS	Co TPPS	mesp-CTS
Co 2p	Co–N	798.0	797.6	-
		786.6	782.1	-
Cl 2p	Cl–Co	196.4	199.6	-
N 1s	N–C= (N=C)	399.8	399.9	-
	N–Co	398.0	398.6	-
	NH <sub>2</sub> –C	398.1	-	397.7
	N=C	400.5	-	400.6
	NH–C=O	400.9	-	400.9
	NH <sub>3</sub> –C	401.5	-	-
C 1s	C=O, O–C–O	287.8	-	288.0
	C–N, C=N,			
	C–O, C–O–C	285.0	284.8	285.0
	C–C, C=C	283.8	283.2	283.6
O 1s	O–S	531.3	532.2	-
	O=S	-	531.8	-

After Co TPPS was grafted onto mesp-CTS (or macp-CTS), the ECD of Co was reduced because the BE of Co increased [ $d(\text{BE}) = +0.4$  and  $+4.5$  eV]. The ECD reduction was the result of the following changes: the ECD of Cl increased because the BE of Cl decreased [ $d(\text{BE}) = -3.2$  eV]. At the same time, the ECD of N in the porphyrin ring increased because the BE of N decreased [ $d(\text{BE}) = -0.1$  and  $-0.6$  eV], the ECD of N in amino groups in Co TPPS/mesp-CTS decreased [ $d(\text{BE}) = +0.4$  eV]. In summary, all of the electron density changes above resulted in a more positive charge on the Co ion in the porphyrin ring after grafting to the support, which indicated that Co TPPS/mesp-CTS(or macp-CTS) would facilitate activation of O<sub>2</sub> more effectively than Co TPPS.

To examine the thermal stability of Co TPPS/mesp-CTS and Co TPPS/macp-CTS, thermogravimetric (TG) and differential scanning calorimetry (DSC) curves were recorded, as shown in Figure 5. There were two steps in their mass processes; the first mass loss step ( $\sim 8.9\%$ ) occurred at a temperature lower than 100 °C, whereas the second mass loss step ( $\sim 6.4\%$ ) occurred between 100–180 °C. The first mass loss step was likely because of the escape of intermolecular water from mesp-CTS or macp-CTS, while the second mass loss step resulted from the decomposition of intramolecular water from mesp-CTS or macp-CTS. The immobilized Co porphyrin did not decompose at 150 °C. This finding was expected, because a previous report indicated that decomposition of cobalt porphyrin required a temperature greater than 370 °C [54].

**Figure 5.** Thermo gravimetric (TG) and differential scanning calorimetry (DSC) analysis curves of Co TPPS/mesp-CTS and Co TPPS/macp-CTS.



### 3.2. Oxidation of Ethylbenzene over Co TPPS/mesp-CTS

Oxidation of ethylbenzene with Co TPPS/mesp-(or macp-)CTS and Co TPPS in the presence of molecular oxygen yielded acetophenone and 1-phenylethanol as the major products, and benzaldehyde, benzoic acid, and bis(1-phenylethyl) ester as the major by-products. All products were identified by GC-MS and chemical analysis data.

The effect of temperature on the oxidation of ethylbenzene over Co TPPS/mesp-CTS was investigated at 130–150 °C (Figure 6A). In general, when the temperature was lower than 140 °C, increasing the reaction temperature increased the catalyst turnover number (TON), enhanced ethylbenzene conversion, and improved the yields of major products. For example, the yields of major products increased from 23.2% (130 °C) to 32.0% (140 °C); however, the yields subsequently decreased as the temperature reached >140 °C. The same rule holds true for the catalyst TON and ethylbenzene conversion. The optimal reaction temperature for the oxidation of ethylbenzene over Co TPPS/mesp-CTS was determined to be 140 °C. At the optimal temperature, the supported catalyst was used to investigate the effects of oxygen pressure on ethylbenzene oxidation. Figure 6B shows that oxygen pressure exerted a pronounced influence on ethylbenzene oxidation. The catalytic activity was greatest at 0.8 MPa, with a conversion rate of 47.1% and acetophenone and 1-phenylethanol yields of 32.0%, and no further enhancement of catalytic activity was achieved at higher oxygen pressures. It is possible that an excessively high oxygen concentration decreases catalyst activity because of chitosan carbonization [55], while an excessively low oxygen concentration inhibits ethylbenzene oxidation. Therefore, the optimal oxidation pressure was determined to be 0.8 MPa.

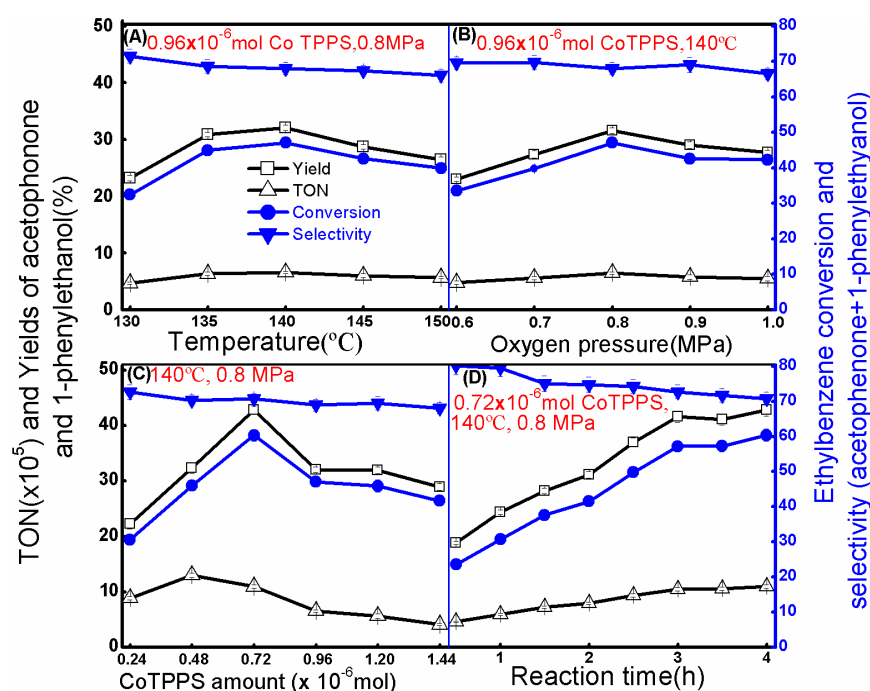


**Figure 6.** Optimization of ethylbenzene oxidation over Co TPPS/mesp-CTS. Reaction conditions: O<sub>2</sub> flow rate = 0.04 m<sup>3</sup>h<sup>-1</sup>. Catalyst turnover number (TON).

Oxidation of ethylbenzene in the absence of a catalyst resulted in a yield of 4.7% (Table 3), indicating that auto-oxidation of ethylbenzene occurred at a very low level. In other words, Co TPPS/mesp-CTS or Co TPPS was responsible for the oxidation of ethylbenzene as described above. Figure 6C shows changes in Co TPPS/mesp-CTS activity with different amounts of the catalyst at the optimal reaction temperature of 140 °C and the optimal pressure of 0.8 MPa. The ethylbenzene conversion rate, catalyst TON, and major product yields often, but not always, increased as the amount

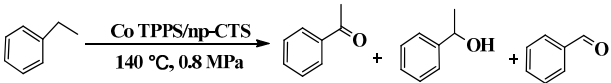
of the catalyst increased; however, when the amount of the catalyst was increased to  $1.44 \times 10^{-6}$  mol, each of these parameters decreased. These results describe the so-called ‘catalyst inhibitor conversion’ phenomenon reported by Black [56] and Guo et al. [57,58], which is known from several auto-oxidation reactions catalyzed by transition metal salts in low polar media.

Figure 6D shows the effect of time on ethylbenzene oxidation. The ethylbenzene conversion rate and the yields of major products increased rapidly from 0–3 h, but increased slowly from 3–4 h. It is likely that the products formed during oxidation covered the surface of the solid catalyst, leading to catalyst activation oppression [59]. Although selectivity (acetophenone and 1-phenylethanol) decreased slowly before the fourth hour, while the catalyst TON increased slightly, these changes were insignificant. Therefore, a 4-h reaction time is optimal for the oxidation of ethylbenzene over Co TPPS/mesp-CTS.

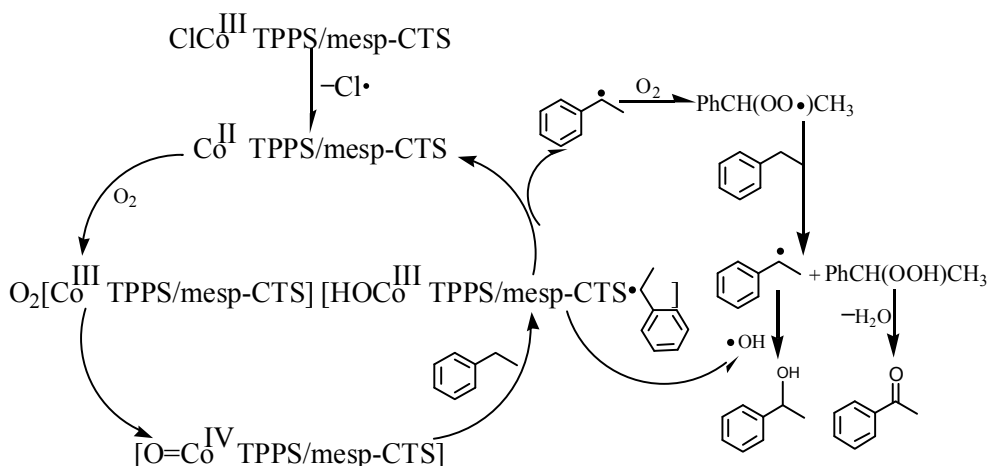
The stability and reusability of a supported catalyst is very important. We report that  $0.96 \times 10$  mol Co TPPS grafted onto 1 g of mesp-CTS can be reused up to four times, on average, for ethylbenzene oxidation, which provided a catalyst TON of  $2.46 \times 10$  and a ketone and alcohol yield of 44.6% (Table 3). These results show that the catalytic performance of the grafted catalyst was better than that of other catalysts, such as Co TPPS and Co TPPS/macp-CTS. These benefits were likely because of the formation of the mesoporous catalyst and axial coordination.

The mechanism of metalloporphyrin-catalyzed oxidations of ethylbenzene by molecular oxygen has been a matter of debate for the past several years, but the primary mechanism is now generally considered to be metalloporphyrin-catalyzed free radical oxidation [60–62]. Several different cobalt porphyrins have been employed as catalysts for the activation of  $O_2$  [41,63–66]. Based on the metalloporphyrin/ $O_2$  system discussed above, a possible catalytic cycle with a high-valent [mesp-CTS/TPPS Co=O] species as the active oxidant is proposed (Scheme 1). Mesp-CTS/TPPS CoCl is reduced to mesp-CTS/TPPS Co by the loss of a chlorine radical. The intermediate reacts immediately with  $O_2$  to form [mesp-CTS/TPPS Co] $_2O_2$ . However, the O–O bond in [mesp-CTS/TPPS Co] $_2O_2$  is homogeneously cleaved by heating, forming an active intermediate, [mesp-CTS/TPPS Co=O]. The [mesp-CTS/TPPS Co=O] promptly abstracts an  $\alpha$ -hydrogen atom from ethylbenzene, producing [mesp-CTS/TPPS CoOH], which forms the hydroxyl radical,  $\cdot OH$ , as well as [mesp-CTS/TPPS Co], which proceeds into the next recycle. The major reaction products, 1-phenylethanol and acetophenone, are generated in radical chain transfer processes; 1-phenylethanol is generated first, followed by acetophenone, as shown in Scheme 1 and Figure 7 (left).

**Table 3.** Comparison of the catalytic performance of Co TPPS/mesp-CTS with that of Co TPPS/macroporous-CTS (macp-CTS) and Co TPPS. <sup>a</sup>

							
Catalyst	Run	TON ( $\times 10^6$ )	Yield (%)	Selectivity (%)			
				-on	-ol	-al	(-ac) + (-es)
Co TPPS/mesp-CTS	1	1.10	42.8	65.4	5.4	3.4	25.8
	2	1.65	50.0	65.4	6.0	3.6	25.0
	3	2.04	43.7	62.4	4.5	3.1	30.0
	4	5.05	42.0	62.5	3.5	3.2	30.8
Average		2.46	44.6	63.9	4.9	3.3	27.9
Co TPPS <sup>b</sup>	1	0.90	34.8	53.3	4.0	3.1	39.6
Co TPPS/macp-CTS <sup>b</sup>	1	0.99	36.8	60.1	4.9	4.0	31.0
No catalyst			4.7	43.3	13.3	8.8	34.6

<sup>a</sup> Yield = acetophenone + 1-phenylethanol; TON = catalyst turnover number; -on: acetophenone; -ol: 1-phenylethanol; -al: benzaldehyde; -ac: benzoic acid; -es: 1-phenylethyl benzoate. Reaction conditions: 0.2 L ethylbenzene, 140 °C, 0.8 MPa,  $0.72 \times 10^{-6}$  mol Co TPPS, 4 h reaction time; <sup>b</sup> Co TPPS could not be recovered; the catalytic performance of recovered Co TPPS/macp-CTS was weakened.



**Scheme 1.** A proposed mechanism for ethylbenzene oxidation over mesoporous chitosan(mesp-CTS) grafted cobalt porphyrin.

Under the optimum oxidation conditions described above, the selectivity (one + ol) and TON obtained from ethylbenzene oxidation over three catalysts are shown in Figure 7. The selectivity for 1-phenylethanol decreased with the reaction time, while the selectivity for acetophenone increased, as shown in Figure 7 (left), which means that 1-phenylethanol was generated first and quickly oxidized into acetophenone (Scheme 1). The selectivity of Co TPPS/mesp-CTS for acetophenone and 1-phenylethanol was higher than that of Co TPPS/macp-CTS and Co TPPS because there were many mesoporous cavities with hydrophilic groups (-OH) and mesopores, which are important factors in mass transport and diffusion, in Co TPPS/mesp-CTS [67,68]. As the mesopores captured ketones and alcohols, dispersal of the freshly generated acetophenone to the other active catalytic site, [mesp-CTS/TPPS Co=O] (Scheme 1), was delayed, which facilitated further oxidation of acetophenone into by-products (al + ac + es). However, Co TPPS/macp-CTS with macropores and Co TPPS had catalytic characteristics different from those of Co TPPS/mesp-CTS. Co TPPS/macp-CTS and Co TPPS had relatively open airways (bigger pores or no pores), which facilitated transportation of acetophenone and 1-phenylethanol to other active catalytic sites and oxidation, and thus provided lower selectivity for the main products (Table 3). This is likely the reason that Co TPPS/mesp-CTS had the highest selectivity to ketones and alcohols, as shown in Figure 7 (right). In our previous work [27,28], Mn TCPP/pd-CTS had better selectivity and yield (one + ol) than Mn TCPP/np-CTS (in fact, Mn TCPP/mesp-CTS). This difference was likely caused by the higher temperature of ethylbenzene oxidation (155 °C), but Mn TCPP/mesp-CTS still showed better ethylbenzene conversion than Mn TCPP/pd-CTS, at least partly because of the catalytic characteristics of the mesoporous catalyst material.

Figure 7 (right) shows that Co TPPS/mesp-CTS, just like Co TPPS/macp-CTS, had better TON and ethylbenzene conversion than Co TPPS, because the Co ion in Co TPPS/mesp-CTS had a more positive charge than that in Co TPPS after the NH<sub>2</sub>-group-coordination of the cobalt porphyrin. In addition, Co TPPS/mesp-CTS showed better selectivity to ketones and alcohols than Co TPPS/macp-CTS, because of the characteristics of the mesoporous catalyst material.

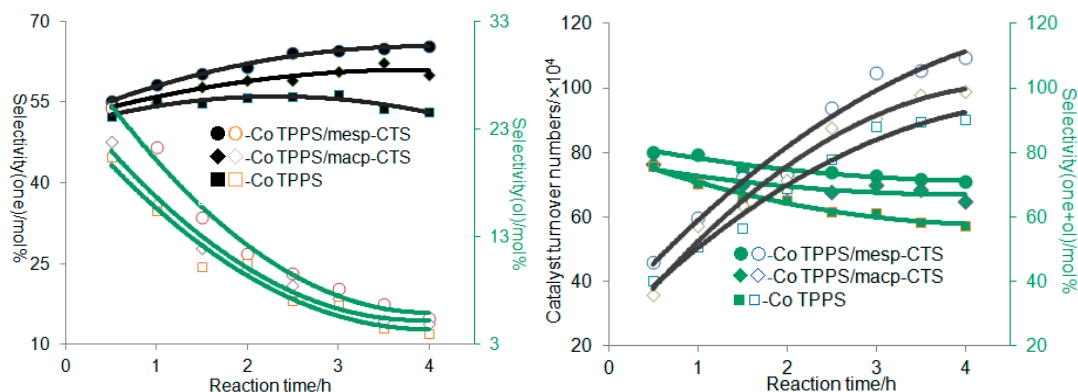


Figure 7. Comparison of the selectivity (one + ol) and TON of three catalysts.

These findings show that mesp-CTS exerts an important influence on the catalytic activity of Co TPPS for oxidation of ethylbenzene because of its characteristic mesopores and axial coordination.

#### 4. Conclusions

In comparison with Co TPPS/macp-CTS and Co TPPS, the moderate biomimetic catalyst Co TPPS/mesp-CTS catalyzed the oxidation of ethylbenzene under mild reaction conditions to provide better selectivity and yields of acetophenone and 1-phenylethanol. The mesoporous action and axial coordination of mesp-CTS to Co TPPS promoted catalytic selectivity (one + ol) and ethylbenzene conversion, which increased yields of ketones and alcohols. These properties stem from the characteristics of the mesoporous catalyst material, Co TPPS/mesp-CTS, which was created by ligating and grafting cobalt porphyrin onto the amino groups of chitosan, and the resulting change in the ECD of the cobalt ion in the catalyst. Immobilization of the catalyst Co TPPS on chitosan to produce Co TPPS/mesp-CTS also increased the catalytic stability of Co TPPS for the oxidation of ethylbenzene.

**Author Contributions:** G.H. and L.Q.M. conceived and designed the experiments; L.Q.M., Y.X.W., H.Z., Y.A.G. and S.J.W. performed the experiments; G.H., L.Q.M. and Y.X.W. analyzed the data; H.Z., Y.A.G. and S.J.W. contributed reagents/materials/analysis tools; G.H. and L.Q.M. wrote the paper.

**Acknowledgments:** This research was supported by the National Natural Science Foundation of China (No. 51363001), the Natural Science Foundation of Guangxi (No. 2014GXNSFDA118009), the Scientific and Technological Project of Guangxi (No. 12118008-12-3), and the Experimental Innovation Project Foundation of Guangxi University, PR China (No. 201510593308).

**Conflicts of Interest:** The authors declare no conflict of interest.

#### References

1. Yang, S.L.; Peng, L.; Huang, P.P.; Wang, X.S.; Sun, Y.B.; Cao, C.Y.; Song, W.G. Nitrogen, phosphorus, and sulfur co-doped hollow carbon shell as superior metal-free catalyst for selective oxidation of aromatic alkanes. *Angew. Chem. Int. Ed.* **2016**, *55*, 4016–4020. [[CrossRef](#)] [[PubMed](#)]
2. Jiang, W.; Yang, J.; Liu, Y.Y.; Ma, J.F. Porphyrin-based mixed-valent Ag(I)/Ag(II) and Cu(I)/Cu(II) networks as efficient heterogeneous catalysts for the azide-alkyne “click” reaction and promising oxidation of ethylbenzene. *Chem. Commun.* **2016**, *52*, 1373–1376. [[CrossRef](#)] [[PubMed](#)]
3. Liu, T.; Cheng, H.Y.; Sun, L.S.; Liang, F.; Zhang, C.; Ying, Z.; Lin, W.W.; Zhao, F.Y. Synthesis of acetophenone from aerobic catalytic oxidation of ethylbenzene over Ti–Zr–Co alloy catalyst: Influence of annealing conditions. *Appl. Catal. A Gen.* **2016**, *512*, 9–14. [[CrossRef](#)]
4. Xie, R.F.; Fan, G.L.; Yang, L.; Li, F. Hierarchical flower-like Co–Cu mixed metal oxide microspheres as highly efficient catalysts for selective oxidation of ethylbenzene. *Chem. Eng. J.* **2016**, *288*, 169–178. [[CrossRef](#)]

5. Selvamani, A.; Selvaraj, M.; Krishnan, P.S.; Gurulakshmi, M.; Shanthi, K. Low temperature vapor phase selective oxidation of ethylbenzene over Ce1–xMnxO<sub>2</sub> nanotubes. *Appl. Catal. A Gen.* **2015**, *495*, 92–103. [[CrossRef](#)]
6. Zhang, Z.Q.; Duan, Y.; Zhang, L.; Yu, M.M.; Li, J. Synthesis, crystal structure of two new Zn(II), Cu(II) porphyrins and their catalytic activities to ethylbenzene oxidation. *Inorg. Chem. Commun.* **2015**, *58*, 53–56. [[CrossRef](#)]
7. Chen, A.B.; Yu, Y.F.; Wang, R.J.; Yu, Y.H.; Zang, W.W.; Tang, P.; Ma, D. Nitrogen-doped dual mesoporous carbon for the selective oxidation of ethylbenzene. *Nanoscale* **2015**, *7*, 14684–14690. [[CrossRef](#)] [[PubMed](#)]
8. Zhao, Q.M.; Chen, K.X.; Zhang, W.S.; Yao, J.; Li, H.R. Efficient metal-free oxidation of ethylbenzene with molecular oxygen utilizing the synergistic combination of NHPI analogues. *J. Mol. Catal. A Chem.* **2015**, *402*, 79–82. [[CrossRef](#)]
9. Li, H.Y.; Ma, H.; Wang, X.H.; Gao, J.; Chen, C.; Shi, S.; Qu, M.J.; Feng, N.; Xu, J. Efficient oxidation of ethylbenzene catalyzed by cobalt zeolitic imidazolate framework ZIF-67 and NHPI. *J. Energy Chem.* **2014**, *23*, 742–746. [[CrossRef](#)]
10. Wang, J.; Liu, H.Y.; Gu, X.M.; Wang, H.H.; Su, D.S. Synthesis of nitrogen-containing ordered mesoporous carbon as a metal-free catalyst for selective oxidation of ethylbenzene. *Chem. Commun.* **2014**, *50*, 9182–9184. [[CrossRef](#)] [[PubMed](#)]
11. Bay, S.; Baumeister, T.; Hashmi, A.S.K.; Röder, T. Safe and fast flow synthesis of functionalized oxazoles with molecular oxygen in a microstructured reactor. *Org. Process Res. Dev.* **2016**, *20*, 1297–1304. [[CrossRef](#)]
12. Hashmi, A.S.; Blanco Jaimes, M.C.; Schuster, A.M.; Rominger, F. From propargylic amides to functionalized oxazoles: Domino gold catalysis/oxidation by dioxygen. *J. Org. Chem.* **2012**, *77*, 6394–6408. [[CrossRef](#)] [[PubMed](#)]
13. Almeida, M.P.D.; Martins, L.M.D.R.S.; Carabineiro, S.A.C.; Lauterbach, T.; Rominger, F.; Hashmi, A.S.K.; Pombeiro, A.J.L.; Figueiredo, J.L. Homogeneous and heterogenised new gold C-scorpionate complexes as catalysts for cyclohexane oxidation. *Catal. Sci. Technol.* **2013**, *3*, 3056–3069. [[CrossRef](#)]
14. Yang, L.; Fan, B.B.; Cui, X.Y.; Shi, X.F.; Li, R.F. Solvent-free aerobic oxidation of ethylbenzene over Mn-containing silylated MgAl layered double hydroxides. *J. Ind. Eng. Chem.* **2015**, *21*, 689–695. [[CrossRef](#)]
15. Chen, Y.; Zhao, S.F.; Liu, Z.G. Influence of the synergistic effect between Co–N–C and ceria on the catalytic performance for selective oxidation of ethylbenzene. *Phys. Chem. Chem. Phys.* **2015**, *17*, 14012–14020. [[CrossRef](#)] [[PubMed](#)]
16. Fu, L.L.; Chen, Y.; Liu, Z.G. Cobalt catalysts embedded in N-doped carbon derived from cobalt porphyrin via a one-pot method for ethylbenzene oxidation. *J. Mol. Catal. A Chem.* **2015**, *408*, 91–97. [[CrossRef](#)]
17. Lv, W.M.; Yang, L.; Fan, B.B.; Zhao, Y.; Chen, Y.F.; Lu, N.Y.; Li, R.F. Silylated MgAl LDHs intercalated with MnO<sub>2</sub> nanowires: Highly efficient catalysts for the solvent-free aerobic oxidation of ethylbenzene. *Chem. Eng. J.* **2015**, *263*, 309–316. [[CrossRef](#)]
18. Wang, R.X.; Gao, B.J.; Jiao, W.Z. A novel method for immobilization of Co tetraphenylporphyrins on P(4VP-co-St)/SiO<sub>2</sub>: Efficient catalysts for aerobic oxidation of ethylbenzenes. *Appl. Surf. Sci.* **2009**, *255*, 4109–4113. [[CrossRef](#)]
19. Shen, D.H.; Ji, L.T.; Liu, Z.G.; Sheng, W.B.; Guo, C.C. Ethylbenzene oxidation over hybrid metalloporphyrin@silica nanocomposite microspheres. *J. Mol. Catal. A Chem.* **2013**, *379*, 15–20.
20. Zhao, M.; Ou, S.; Wu, C.D. Porous metal-organic frameworks for heterogeneous biomimetic catalysis. *Acc. Chem. Res.* **2014**, *47*, 1199–1207. [[CrossRef](#)] [[PubMed](#)]
21. Jing, J.Y.; Zhang, Y.; Feng, J.; Li, W.Y.; Yu, W.W. Facile preparation and high performance of magnetically separable metalloporphyrin. *Chem. Eng. J.* **2015**, *263*, 385–391. [[CrossRef](#)]
22. Brule, E.; Miguel, Y.R.; Hiic, K.K. Chemoselective epoxidation of dienes using polymer-supported manganese porphyrin catalysts. *Tetrahedron* **2004**, *60*, 5913–5918. [[CrossRef](#)]
23. Mukherjee, M.; Ray, A.R. Biomimetic oxidation of l-arginine with hydrogen peroxide catalyzed by the resin-supported iron (III) porphyrin. *J. Mol. Catal. A Chem.* **2007**, *266*, 207–214. [[CrossRef](#)]
24. Zhang, W.J.; Jiang, P.P.; Wang, Y.; Zhang, J.; Zheng, J.W.; Zhang, P.B. Selective oxidation over a metalloporphyrinic metal–organic framework catalyst and insights into the mechanism of bicarbonate ion as co-catalyst. *Chem. Eng. J.* **2014**, *257*, 28–35. [[CrossRef](#)]



25. Kumar, D.; Latifi, R.; Kumar, S.; Rybak-Akimova, E.V.; Sainna, M.A.; de Visser, S.P. Rationalization of the barrier height for p-Z-styrene epoxidation by iron(IV)-oxo porphyrin cation radicals with variable axial ligands. *Inorg. Chem.* **2013**, *52*, 7968–7979. [[CrossRef](#)] [[PubMed](#)]
26. Song, W.J.; Ryu, Y.O.; Song, R.; Nam, W. Oxoiron(IV) porphyrin p-cation radical complexes with a chameleon behavior in cytochrome P450 model reactions. *J. Biol. Inorg. Chem.* **2005**, *10*, 294–304. [[CrossRef](#)] [[PubMed](#)]
27. Huang, G.; Yuan, R.X.; Peng, Y.; Chen, X.F.; Zhao, S.K.; Wei, S.J.; Guo, W.X.; Chen, X. Oxygen oxidation of ethylbenzene over manganese porphyrin is promoted by the axial nitrogen coordination in powdered chitosan. *RSC Adv.* **2016**, *6*, 48571–48579. [[CrossRef](#)]
28. Zeng, K.; Huang, G.; Yuan, R.X.; Wang, W.L.; Guo, Y.A.; Zhao, S.K. Catalysis of nano-porous chitosan grafted manganese tetra(p-carboxylphenyl)porphyrin for oxidation of ethylbenzene. *J. Guangxi Univ. (Nat. Sci. Ed.)* **2015**, *40*, 505–513.
29. Cai, J.L.; Huang, G.; Mo, L.Q.; Wei, Y.X.; Guo, Y.A. Catalysis of chitosan-supported cobalt tetrakis(p-sulphophenyl)porphyrin for oxidation of ethylbenzene. *J. Guangxi Univ. (Nat. Sci. Ed.)* **2014**, *39*, 1385–1392.
30. Adler, A.D.; Longo, F.R.; Finarelli, J.D.; Goldmacher, J.; Assour, J.; Korssakow, L. A simplified synthesis for meso-tetraphenylporphin. *J. Org. Chem.* **1967**, *32*, 476. [[CrossRef](#)]
31. Haber, J.; Kłosowski, M.; Połtowicz, J. Co-oxidation of styrene and iso-butylaldehyde in the presence of polyaniline-supported metalloporphyrins. *J. Mol. Catal. A Chem.* **2003**, *201*, 167–178. [[CrossRef](#)]
32. Rorrer, G.L.; Hsien, T.Y.; Way, J.D. Synthesis of porous-magnetic chitosan beads for removal of cadmium ions from waste water. *Ind. Eng. Chem. Res.* **1993**, *32*, 2170–2178. [[CrossRef](#)]
33. Huang, G.; Xiang, F.; Li, T.M.; Jiang, Y.X.; Guo, Y.A. Selective oxidation of toluene over the new catalyst cobalt tetra (4-hydroxyl) phenylporphyrin supported on zinc oxide. *Catal. Commun.* **2011**, *12*, 886–889. [[CrossRef](#)]
34. Huang, G.; Mo, L.Q.; Cai, J.L.; Cao, X.; Peng, Y.; Guo, Y.A.; Wei, S.J. Environmentally friendly and efficient catalysis of cyclohexane oxidation by iron meso-tetrakis(pentafluorophenyl)porphyrin immobilized on zinc oxide. *Appl. Catal. B Environ.* **2015**, *162*, 364–371. [[CrossRef](#)]
35. Claire, M.T.; Chai, S.H.; Dai, S.; Unocic, K.A.; Alamgir, F.M.; Agrawal, P.K.; Jones, C.W. Tuning of higher alcohol selectivity and productivity in CO hydrogenation reactions over K/MoS<sub>2</sub> domains supported on mesoporous activated carbon and mixed MgAl oxide. *J. Catal.* **2015**, *324*, 88–97. [[CrossRef](#)]
36. Singh, V.; Tiwari, A.; Tripathi, D.N.; Sanghi, R. Microwave enhanced synthesis of chitosan-graft-polyacrylamide. *Polymer* **2006**, *47*, 254–260. [[CrossRef](#)]
37. Lim, S.H.; Hudson, S.M. Synthesis and antimicrobial activity of a water-soluble chitosan derivative with a fiber-reactive group. *Carbohydr. Res.* **2004**, *339*, 313–319. [[CrossRef](#)] [[PubMed](#)]
38. Zhang, Y.H.; Chen, D.M.; He, T.J.; Liu, F.C. Raman and infrared spectral study of meso-sulfonatophenyl substituted porphyrins (TPPS<sub>n</sub>, n=1, 2A, 2O, 3, 4). *Spectrochim. Acta Part A* **2003**, *59*, 87–101. [[CrossRef](#)]
39. Rong, Y.; Chen, P.; Liu, M. Self-assembly of water-soluble TPPS in organic solvents: From nanofibers to mirror imaged chiral nanorods. *Chem. Commun.* **2013**, *49*, 10498–10500. [[CrossRef](#)] [[PubMed](#)]
40. Orihara, Y.; Uo, M.; Inoue, H.; Makishima, A.; Tani, T. Preparation and spectroscopy of lead-tin fluorophosphate glass doped with TPPS and TPPS-Sn. *Phys. Chem.* **1996**, *100*, 1582–1587. [[CrossRef](#)]
41. Shen, L.L.; Qu, R.; Shi, H.J.; Huang, F.; An, Y.L.; Shi, L.Q. A biocompatible cobaltporphyrin-based complex micelle constructed via supramolecular assembly for oxygen transfer. *Biomater. Sci.* **2016**, *4*, 857–862. [[CrossRef](#)] [[PubMed](#)]
42. Annoni, E.; Pizzotti, M.; Ugo, R.; Quici, S.; Morotti, T.; Casati, N.; Macchi, P. The effect on E-stilbazoles second order NLO response by axial interaction with M(II),10,15,20-tetraphenyl porphyrinates (M = Zn, Ru, Os); a new crystalline packing with very large holes. *Inorg. Chim. Acta* **2006**, *359*, 3029–3041. [[CrossRef](#)]
43. Yan, Y.; Yao, P.P.; Mu, Q.; Wang, L.; Mu, J.; Li, X.Q.; Kang, S.Z. Electrochemical behavior of amino-modified multi-walled carbon nanotubes coordinated with cobalt porphyrin for the oxidation of nitric oxide. *Appl. Surf. Sci.* **2011**, *258*, 58–63. [[CrossRef](#)]
44. Marco, J.F.; Gancedo, J.R.; Gracia, M.; Gautier, J.L.; Rios, E.I.; Palmer, R.; Greaves, C.; Berry, F.J. Cation distribution and magnetic structure of the ferrimagnetic spinel NiCo<sub>2</sub>O<sub>4</sub>. *J. Mater. Chem.* **2001**, *11*, 3087–3093. [[CrossRef](#)]

45. Liang, H.W.; Wei, W.; Wu, Z.S.; Feng, X.L.; Mullen, K. Mesoporous metal-nitrogen-doped carbon electrocatalysts for highly efficient oxygen reduction reaction. *J. Am. Chem. Soc.* **2013**, *135*, 16002–16005. [[CrossRef](#)] [[PubMed](#)]
46. Liu, J.; Zheng, L.C.; Li, Y.W.; Free, M.; Yang, M.Z. Adsorptive recovery of palladium(II) from aqueous solution onto cross-linked chitosan/montmorillonite membrane. *RSC Adv.* **2016**, *6*, 51757–51767. [[CrossRef](#)]
47. Roy, P.S.; Samanta, A.; Mukherjee, M.; Roy, B.; Mukherjee, A. Designing novel pH-induced chitosan–gum odina complex coacervates for colon targeting. *Ind. Eng. Chem. Res.* **2013**, *52*, 15728–15745. [[CrossRef](#)]
48. Maachou, H.; Genet, M.J.; Aliouche, D.; Dupont-Gillainb, C.C.; Rouxhet, P.G. XPS analysis of chitosan–hydroxyapatite biomaterials: From elements to compounds. *Surf. Interface Anal.* **2013**, *45*, 1088–1097. [[CrossRef](#)]
49. Berner, S.; Lidbaum, H.; Ledung, G.; Ahlund, J.; Nilson, K.; Schiessling, J.; Gelius, U.; Backvall, J.E.; Puglia, C.; Oscarsson, S. Electronic and structural studies of immobilized thiol-derivatized cobalt porphyrins on gold surfaces. *Appl. Surf. Sci.* **2007**, *253*, 7540–7548. [[CrossRef](#)]
50. Xin, L.; Yang, F.; Rasouli, S.; Qiu, Y.; Li, Z.F.; Uzunoglu, A.; Sun, C.J.; Liu, Y.Z.; Ferreira, P.; Li, W.Z.; et al. Understanding Pt nanoparticle anchoring on graphene supports through surface functionalization. *ACS Catal.* **2016**, *6*, 2642–2653. [[CrossRef](#)]
51. Varadwaj, G.B.B.; Rana, S.; Parida, K.; Nayak, B.B. A multi-functionalized montmorillonite for co-operative catalysis in one-pot Henry reaction and water pollution remediation. *J. Mater. Chem. A* **2014**, *2*, 7526–7534. [[CrossRef](#)]
52. Han, M.G.; Cho, S.K.; Oh, S.G.; Im, S.S. Preparation and characterization of polyaniline nanoparticles synthesized from DBSA micellar solution. *Synth. Met.* **2002**, *126*, 53–60. [[CrossRef](#)]
53. Li, Y.; Zhang, J.; Xu, C.; Zhou, Y.F. Crosslinked chitosan nanofiber mats fabricated by one-step electrospinning and ion-imprinting methods for metal ions adsorption. *Sci. China Chem.* **2015**, *59*, 95–105. [[CrossRef](#)]
54. Fidalgo-Marijuan, A.; Barandika, G.; Bazan, B.; Urtiaga, M.K.; Arriortua, M.I. Thermal stability and crystallochemical analysis for Co<sup>II</sup>-based coordination polymers with TPP and TPPS porphyrins. *CrystEngComm* **2013**, *15*, 4181–4188. [[CrossRef](#)]
55. Huang, G.; Luo, J.; Deng, C.C.; Guo, Y.A.; Zhao, S.K.; Zhou, H.; Wei, S. Catalytic oxidation of toluene with molecular oxygen over manganese tetraphenylporphyrin supported on chitosan. *Appl. Catal. A Gen.* **2008**, *338*, 83–86. [[CrossRef](#)]
56. Black, J.F. Metal-catalyzed autoxidation. The unrecognized consequences of metal-hydroperoxide complex formation. *J. Am. Chem. Soc.* **1978**, *100*, 527–535. [[CrossRef](#)]
57. Guo, C.C.; Liu, Q.; Wang, X.T.; Hu, H.Y. Selective liquid phase oxidation of toluene with air. *Appl. Catal. A Gen.* **2005**, *282*, 55–59. [[CrossRef](#)]
58. Guo, C.C.; Liu, X.Q.; Liu, Y.; Liu, Q.; Chu, M.F.; Zhang, X.B. Studies of simple  $\mu$ -oxo-bisiron(III)porphyrin as catalyst of cyclohexane oxidation with air in absence of cocatalysts or coreductants. *J. Mol. Catal. A Chem.* **2003**, *192*, 289–294. [[CrossRef](#)]
59. Kasaikina, O.T.; Kortenska, V.D.; Kartasheva, Z.S.; Kuznetsova, G.M.; Maximova, T.V.; Sirota, T.V.; Yanishlieva, N.V. Hydrocarbon and lipid oxidation in micro heterogeneous systems formed by surfactants or nanodispersed Al<sub>2</sub>O<sub>3</sub>, SiO<sub>2</sub> and TiO<sub>2</sub>. *Colloids Surf. A Physicochem. Eng. Aspects* **1999**, *149*, 29–38. [[CrossRef](#)]
60. Evans, S.; Smith, J.R.L. The oxidation of ethylbenzene and other alkylaromatics by dioxygen catalysed by iron(III) tetrakis(pentafluorophenyl)porphyrin and related iron porphyrins. *J. Chem. Soc. Perkin Trans.* **2000**, *2*, 1541–1552. [[CrossRef](#)]
61. Evans, S.; Smith, J.R.L. The oxidation of ethylbenzene by dioxygen catalysed by supported iron porphyrins derived from iron(III) tetrakis(pentafluorophenyl)porphyrin. *J. Chem. Soc. Perkin Trans* **2001**, *2*, 174–180. [[CrossRef](#)]
62. Lyons, J.E.; Ellis, P.E.; Myers, H.K. Halogenated metalloporphyrin complexes as catalysts for selective reactions of acyclic alkanes with molecular oxygen. *J. Catal.* **1995**, *155*, 59–73. [[CrossRef](#)]
63. Zhou, X.T.; Ji, H.B. Highly efficient oxidative cleavage of carbon-carbon double bond over meso-tetraphenyl cobalt porphyrin catalyst in the presence of molecular oxygen. *Chin. J. Chem.* **2012**, *30*, 2103–2108. [[CrossRef](#)]
64. Scherson, D.A.; Gupta, S.L.; Fierro, C.; Yeager, E.B.; Kordesch, M.E.; Eldridge, J.; Hoffman, R.W.; Blue, J. Cobalt tetramethoxyphenyl porphyrin-emission mossbauer spectroscopy and O<sub>2</sub>, reduction electrochemical studies. *Electrochim. Acta.* **1983**, *28*, 1205–1209. [[CrossRef](#)]

65. Walker, F.A. ESR studies of Co(II) tetraphenylporphyrins and their oxygen adducts: Complex formation with aromatic molecules and sterically hindered lewis base. *J. Magn. Reson.* **1974**, *15*, 201–218. [[CrossRef](#)]
66. Weselucha-Birczynska, A.; Nakamoto, K.; Proniewicz, L.M. Simultaneous observation of  $\nu(\text{O}-\text{O})$ ,  $\nu(\text{Co}-\text{O}_2)$  and  $\delta(\text{CoOO})$  in resonance Raman spectra of five- and six-coordinate dioxygen adducts of Co(TPP-d<sub>8</sub>). *J. Mol. Struct.* **1992**, *275*, 95–103. [[CrossRef](#)]
67. Lee, C.H.; Lin, H.C.; Cheng, S.H.; Lin, T.S.; Mou, C.Y. Hydroxo-bridged dinuclear cupric complexes encapsulated in various mesoporous silicas to mimic the catalytic activity of catechol oxidases: Reactivity and selectivity study. *J. Phys. Chem. C* **2009**, *113*, 16058–16069. [[CrossRef](#)]
68. Feng, X.; Sheng, N.; Liu, Y.B.; Che, X.B.; Chen, D.; Yang, C.H.; Zhou, X.G. Simultaneously enhanced stability and selectivity for propene epoxidation with H<sub>2</sub> and O<sub>2</sub> on Au catalysts supported on nano-crystalline mesoporous TS-1. *ACS Catal.* **2017**, *7*, 2668–2675. [[CrossRef](#)]



© 2018 by the authors. Licensee MDPI, Basel, Switzerland. This article is an open access article distributed under the terms and conditions of the Creative Commons Attribution (CC BY) license (<http://creativecommons.org/licenses/by/4.0/>).